arXiv:astro-ph/9611141v1 18 Nov 1996

Globular Cluster Luminosity Functions and the Hubble Constant from WFPC2 Imaging: The Dominant Group Elliptical NGC 5846[1]

Duncan A. Forbes
Lick Observatory, University of California, Santa Cruz, CA 95064
and
School of Physics and Space Research, University of Birmingham, Edgbaston, Birmingham B15 2TT, United Kingdom
Electronic mail: forbes@lick.ucsc.edu

Jean P. Brodie
Lick Observatory, University of California, Santa Cruz, CA 95064
Electronic mail: brodie@lick.ucsc.edu

John Huchra
Harvard–Smithsonian Center for Astrophysics, 60 Garden Street, Cambridge, Massachusetts 02138
Electronic mail: huchra@cfa.harvard.edu

ABSTRACT

The *Hubble Space Telescope's* Wide Field and Planetary Camera 2 (WFPC2) has several advantages over ground–based observations for the study of globular cluster luminosity functions (GCLFs) and distance determination. Here we present WFPC2 data on the globular clusters associated with NGC 5846. This giant elliptical is the dominant galaxy in a small, compact group located $\sim$ 13 Mpc beyond the Virgo cluster. We have detected over 1200 globular clusters in three (central, north and south) separate pointings. The luminosity function in each of these pointings are statistically the same, indicating that the mean luminosity (mass) does not vary between $\sim$ 3 and 30 kpc from the galaxy center. This suggests that dynamical friction and bulge shocking destruction processes are insignificant. We have fit a Gaussian and t_5 profile to the GCLF (of the combined pointings) and find that it is well represented by a turnover magnitude of m_V^0 = 25.05 $\pm$ 0.10 and a dispersion of $\sigma = 1.34 \pm 0.06$. Our 50% completeness level is $\sim$ 1 mag fainter than the turnover. After applying a metallicity correction to the 'universal' GCLF turnover magnitude, we derive a distance modulus of (m–M) = 32.32 $\pm$ 0.23. For a group velocity V_{CMB} = 1883 $\pm$ 28 km s^{-1}, the Hubble constant is $H_\circ$ = 65 $\pm$ 8 km s^{-1} Mpc^{-1}.

---

[1] Based on observations with the NASA/ESA *Hubble Space Telescope*, obtained at the Space Telescope Science Institute, which is operated by AURA, Inc., under NASA contract NAS 5–26555

1. Introduction

Significant advances have been made recently in the measurement of extragalactic distances, which are summarized in the proceedings of the *Space Telescope Science Institute* workshop on 'The Extragalactic Distance Scale'. As expected, the *Hubble Space Telescope* (HST) has contributed to more than one of the distance determination methods. Most of the published results, so far, relate to the Cepheid Variable method (e.g. Freeman *et al.* 1994; Mould *et al.* 1995; Kelson *et al.* 1996) and the globular cluster luminosity function (GCLF) method (e.g. Baum *et al.* 1995; Whitmore *et al.* 1995; Forbes 1996a,b). In the case of the GCLF method, the 'standard candle' is the magnitude of the turnover, or peak, in the luminosity function of a galaxy's globular clusters. The method can be applied to both spiral and elliptical galaxies. The main assumption inherent in this method is that the GCLF turnover magnitude is constant (with a value of $M_V^0 \sim -7.5$). Observations with the HST improve the precision of GCLF studies in several ways; namely, accurate photometry to fainter magnitudes than typically obtained from the ground, no blending of globular clusters in the central galaxy regions and very low contamination as most stars and galaxies can be easily excluded. This improved precision helps to address the issue of a universal GCLF and provide an independent estimate of the Hubble constant.

In this paper we present a GCLF of NGC 5846 from Wide Field and Planetary Camera 2 (WFPC2) observations. NGC 5846 is a giant elliptical galaxy at the center of a small, compact group of galaxies. Extended X–ray emission from hot gas has been detected out to ~ 100 kpc (Biermann, Kronberg & Schmutzler 1989). The inferred virial mass and cooling flow rate are similar to those of M87. Harris (1991) lists a GC specific frequency (relative richness) of $S_N = 2.6 \pm 1.9$, which is somewhat low for an elliptical galaxy and much less than that for M87 ($S_N = 14 \pm 3$). The distance to NGC 5846 is about 30 Mpc, which places it ~ 13 Mpc beyond the Virgo cluster. It lies about 30 degrees on the sky from Virgo, and out of the plane of the local supercluster. These features make it particularly interesting for constraining galaxy bulk flows. In this paper we will focus on the GCLF of NGC 5846 and use it to derive the galaxy's distance modulus. Our WFPC2 imaging consists of three separate pointings which allows us to explore the variation of the luminosity function with galactocentric distance. A future paper (Forbes *et al.* 1997) will explore the color and spatial properties of the NGC 5846 GC system.

2. Observations and Data Reduction

We obtained F555W (V) and F814W (I) images of NGC 5846 at three separate pointings (central, north and south) with the WFPC2 of HST. The data were obtained in 1996 April 14 for the central pointing, April 28 for the ~ 1.5 arcmin north pointing and April 24 for the ~ 2.5 arcmin south pointing. The exposure times were all 900, 1300 secs for the F555W, and 900, 1400 secs for F814W. After alignment, each pair of images were combined using the STSDAS task *gcombine* weighted by exposure time.

The detection of GCs was carried out using DAOPHOT (Stetson 1987) in a manner similar to that described in Forbes *et al.* (1996). A signal-to-noise threshold of 4 per pixel, 'sharpness' range of 0.55 to 1.1 and roundness of -1 to 1 was used for the initial detection of GCs. The two filters were processed separately, so that the F555W and F814W GC candidate lists are independent. As we measured 2 pixel radius aperture magnitudes, an aperture correction to a $0.5''$ aperture was applied based on Table 2 of Holtzman *et al.* (1995), i.e. 0.39 and 0.19 for the F555W Planetary Camera (PC) and Wide Field Camera (WFC) CCDs, and 0.54 and 0.23 for the F814W PC and WFC CCDs. We then used the transformations from Table 7 of Holtzman *et al.* (1996), for a gain setting of 7, to convert magnitudes into the standard Johnson–Cousins V, I system. Finally we corrected for Galactic extinction of $A_V = 0.11$ and $A_I = 0.05$ (Faber *et al.* 1989).

The candidate GC lists were then compared to the known positions and counts of hot pixels. When the photometry would be affected by more than 2% we excluded those GCs from the list (typically half a dozen per CCD). A FWHM size selection was also made. In this case objects with sizes less than 1 pixel or greater than 3 pixels were excluded. Visually objects with FWHM size > 3 pixels are clearly galaxies. From a simulation of the large Galactic GC Omega Cen (Grillmair 1995) we expect all GCs at the distance of NGC 5846 to be well within the 3 pixel size limit. The typical GC in our data has a FWHM size ~ 1.6 pixels. Finally a visual check is performed on all images to see if any obvious spurious objects remain. After these criteria have been applied, we are confident that the contamination from cosmic rays, hot pixels, foreground stars and background galaxies is small (order of a few percent) in our object list. An example of our final selection of GCs is given in Fig. 1 (Plate ***), in which we show part of a Wide Field Camera CCD with the selected GCs indicated.

It is important to note that we have not made any selection based on color. In this paper we will use only the V band data (which is of higher signal-to-noise than the I band data). The color–selected sample suggests a bimodal V–I color distribution. Examination of the luminosity function of the blue and red subsamples reveals that there is no statistical difference between them (as given by a K–S test). Thus we can analyze the total V band data irrespective of color.

3. Modeling

3.1. Completeness Function

It is crucial for GCLF studies to quantify the ability of DAOPHOT to detect GCs as a function of magnitude (called the completeness function). This is achieved by simulating GCs and then re–running DAOPHOT with the same detection parameters and selection criteria as for the real data. As discussed below, we find no statistical difference between the fraction of actual detected GCs in all three pointings. This indicates that both the intrinsic GCLF *and* the completeness function do not vary from one pointing to another. We have chosen to carry out the simulation on WFC CCD 3 of the north pointing. We simulated a total of 1000 artificial GCs with V > 25. The fraction of detected GCs compared to those created, in 0.1 mag bins, gives the completeness function which is shown in Fig. 2a.

We find that all GCs brighter than V ∼ 25 were detected, whereas at V = 25.95 we are 50% incomplete. The profile shape is similar to that determined by Forbes (1996a) from short exposure time WFPC2 data of NGC 4365, and our 50% incompleteness level is close to that expected based with our improved signal-to-noise data. For the subsequent analysis the completeness function is set to zero for magnitudes fainter than V = 25.95 in order to avoid incompleteness corrections larger than a factor of two.

The completeness function shown in Fig. 2a is appropriate for the WFC CCDs. The PC CCD is expected to have a lower point source sensitivity by ∼0.3 mags given its smaller pixels (Burrows *et al.* 1993). We have also simulated 1000 artificial GCs in a PC CCD and derived its completeness function. It is similar in shape to the WFC function but shifted to brighter magnitudes as expected. We have decided to crudely correct the PC magnitude data by the ratio of the WFC to PC completeness functions, so that the PC data resembles the WFC data. In this paper we will not use data from the central PC pointing as there is some filamentary dust present but we will use the north and south PC pointings.

3.2. Photometric Errors

Photometric, or measurement, errors are also important in GCLF studies. These can cause a shift of the GCLF peak to brighter magnitudes, as some of the fainter GCs, with relatively large errors, move into brighter magnitude bins. This 'bin jumping' effect is described in detail by Secker & Harris (1993) and taken into account in their maximum likelihood technique. The DAOPHOT determined errors are fit with an exponential of the form:

$$\text{p.e.} = \exp\left[a\,(V - b)\right]$$

The photometric error and the fit as a function of V magnitude are shown in Fig. 2b. There is no appreciable difference between the WFC and PC CCD photometric errors. Typical photometric errors are ± 0.05 mag at V = 24. These photometric errors (from DAOPHOT) are similar to those found by comparing the input and measured magnitudes of GCs from simulations.

3.3. Background Contamination

Ground–based GC studies are seriously affected by contamination. In typical $\sim 1''$ seeing conditions, foreground stars and background galaxies can make up to half of any GC candidate list based solely on magnitude (e.g. Perelmuter, Brodie & Huchra 1995). Our situation is significantly improved as most stars and galaxies can be easily identified with the high spatial resolution of WFPC2. We typically exclude 2–4 stars per CCD, which is similar to that expected from high Galactic latitude star counts (see Elson & Santiago 1996) for the range 20 < V < 26. In order to quantify the number of background galaxies to V = 26 we have re–run DAOPHOT with the same detection parameters on a 2400 sec WFPC2 image from the Medium Deep Survey (MDS; Forbes *et al.* 1994). In particular the threshold is still set at 4σ (after determining the appropriate background noise in the MDS image), and we exclude objects with FWHM sizes $<$ 1 pixel and $>$ 3 pixels. No color selection is applied. We find that the number of compact galaxies is insignificant for magnitudes V $<$ 25. Between V = 25 and 25.95 (the 50% incompleteness level), the number of contaminating compact galaxies in our sample approaches 20 per WFPC2 field-of-view. The luminosity function for background unresolved objects is shown in Fig. 3.

4. Results and Discussion

As stated earlier, we will not discuss any results for GCs in the PC CCD of the central pointing. For GCs located on the PC CCD in the other two pointings we have corrected their luminosity function so that the PC probes to a similar depth as the WFC CCDs. A consistency check on this correction is provided by Fig. 4. Here we show the cumulative fraction of actual detected GCs in the central, north and south pointings (WFC CCDs only) compared to that of the north plus south pointing for the PC CCDs (after applying the correction discussed in section 3.1). This figure shows that the detection fraction, as a function of V magnitude, is similar between the PC and WFC CCDs. There are no GCs brighter than V = 23 in the PC CCDs and at magnitudes fainter than V = 25.5 background galaxies become a strong contaminant. Including the GCs from the PC CCDs with the WFC CCDs gives over 1200 GCs within our 50% completeness limit.

Forbes *et al.* (1996) showed that the surface density of GCs tends to flatten off in log space near the galaxy center. The 'core radius' of the GC system ranges from 1 kpc for small ellipticals to $\sim$ 5 kpc for giant ellipticals. They suggested that this core radius was *not* due to a destruction process. However they only had a single central pointing available to them. Here we can critically examine the issue of GC destruction processes. It has been suggested that dynamical friction and bulge shocking may operate in the central regions of galaxies (e.g. Aguliar, Hut & Ostriker 1988; Murray & Lin 1992). Dynamical friction will preferentially destroy high mass GCs, and bulge shocking the low density (low mass) ones. Thus we might expect to see a variation in the luminosity function (i.e. a deficit in bright or faint GCs respectively) with galactocentric radius. Examination of Fig. 4 shows that the detected fraction of GCs is similar for all three pointings. This is confirmed statistically by a K–S test which indicates that each pointing is consistent with having been drawn from the same parent population. This implies that the completeness function *and* the intrinsic luminosity function *do not* vary between the three pointings. The WFC pointings range from about 0.3 to 3 arcminutes (3–30 kpc) in galactocentric radius. Thus we confirm the suggestion of Forbes *et al.* (1996) that GC destruction does not appear to be operating in the central regions of elliptical galaxies and therefore that the present day GC system reflects the properties of the GCs as they were formed.

As in previous work (Forbes 1996a,b), we have used the maximum likelihood technique of Secker & Harris (1993) to accurately determine the GCLF peak magnitude and dispersion. This technique is designed to take proper account of detection incompleteness at faint magnitudes, photometric error and background contamination. The fitting procedure does not use binned data but rather treats all data points individually. We fit both Gaussian and t_5 profiles (Secker 1992). After fitting the GCLF for the Wide Field Camera data set, we find the best estimate and uncertainty of a Gaussian profile to be $m_V^0 = 25.03 \pm 0.10$ and $\sigma = 1.29 \pm 0.06$. These errors represent the collapsed one–dimensional confidence limits for one standard deviation. An increase in the photometric errors to the upper envelope of Fig. 2b changes m_V^0 and σ by less than 1%. In Fig. 5 we show the probability contours for the Gaussian fit. The dispersion for the t_5 profile is $\sigma_t = 1.01$, which is theoretically related to the Gaussian dispersion by $\sigma_G \sim 1.28\sigma_t$. We note that NGC 5846 has a similar t_5 dispersion to the Milky Way GC system ($\sigma_t \sim 1.1$) and somewhat less than is typical for Virgo ellipticals (Secker & Harris 1993). If the GCs on the two PC CCDs are included in the GCLF, then the turnover magnitude is fainter by $\sim$ 0.1 mag and the dispersion increases by 0.05 mag. For a t_5 profile, the turnover is $\sim$ 0.1 mag brighter. The best–fit Gaussian profile is superposed over a binned GCLF in Fig. 6. Note that the actual fitting procedure does not use binned data. For our field-of-view, we have detected about 80% of all expected GCs, i.e. $\sim$ 20% are too faint. Our 50% completeness level is about 1 mag fainter than the turnover and so the bias of the type discussed by Secker & Harris (1992) is minimal. From their figure 6 we have included a correction of 0.05

mag in the turnover (making it fainter) and 0.04 in the dispersion (making it larger). The bias corrected results are given in Table 1.

We calculate the distance modulus from the turnover magnitude assuming the 'universal value' for the turnover is $M_V^0 = -7.62$ with an external error of ± 0.2 (Sandage & Tammann 1995). This universal value is then made fainter by a metallicity–based correction following Ashman, Conti & Zepf (1995). In the absence of a spectroscopic metallicity for the GC system, we can estimate the metallicity from the mean color. Combining our data from the three pointings gives a mean V–I of ~ 1.15. This corresponds roughly to [Fe/H] = –0.29 (Couture, Harris & Allwright 1990), and therefore a correction of $\Delta M_V^0 \sim 0.35$ is required. The resulting distance moduli from the Gaussian and t_5 fits are also given in Table 1. We estimate the error on the distance modulus to be the quadrature sum of the following errors: photometric zeropoint (0.05), charge transfer efficiency effects (0.03), aperture correction (0.03), extinction correction (0.02), variation in M_V^0 (0.2) and variation in m_V^0 (0.10). The error associated with the metallicity correction of Ashman *et al.* (1995) is dominated by the error in M_V^0. These errors give a total of 0.23 magnitudes. Taking the average of the fits, we find (m–M) = 32.32 ± 0.23 and a distance of 29 ± 3.3 Mpc. NGC 5846 is the dominant elliptical in the group and lies at the center of the X–ray emission. It's velocity is within 30 km s^{-1} of the mean velocity for 35 galaxies in the group. Thus, for the corrected recession velocity of NGC 5846, we have adopted the group velocity with respect to the cosmic microwave background, i.e. $V_{CMB} = 1883 \pm 28$ km s^{-1} (Faber *et al.* 1989). For a distance modulus of 32.32 ± 0.23, the resulting Hubble constant is 65 ± 8 km s^{-1} Mpc^{-1}. This calculation assumes that any correction for bulk flows affecting NGC 5846 is small, which is reasonable given that NGC 5846 lies $\sim$ 13 Mpc beyond Virgo (see figure 5 of Jacoby *et al.* 1992).

5. Conclusions

Here we present deep WFPC2 V band images of the giant elliptical NGC 5846, observed in three separate pointings. About 1200 globular clusters are detected in the three pointings, with a 50% completeness limit of V = 25.95. This limit is about 1 magnitude beyond the expected turnover in the globular cluster luminosity function (GCLF) and implies we are missing only the faintest $\sim$ 20% of globular clusters in our field-of-view. We find that the GCLFs are statistically the same over galactocentric radii from $\sim$ 3–30 kpc. This places constraints on the destruction of globular clusters via dynamical friction or bulge shocking as these would be expected to preferentially remove the high or low mass globulars respectively.

We have fit the combined GCLF with both Gaussian and t_5 profiles, using the maximum likelihood analysis of Secker & Harris (1993). The GCLF is well represented by a turnover magnitude of $m_V^0 = 25.05 \pm 0.1$ and dispersion $\sigma = 1.34 \pm 0.06$ (the two fitting profiles give similar results). This demonstrates that a turnover magnitude, accurate to 10%, can be determined from WFPC2 data out to $\sim$ 30 Mpc (or 13 Mpc beyond the distance of Virgo). The distance modulus for NGC 5846 is (m–M) = 32.32 ± 0.23, assuming $M_V^0 = -7.62$ and after applying a metallicity correction from Ashman *et al.* (1995). Adopting the NGC 5846 group velocity, with respect to the cosmic microwave background of 1883 km s^{-1}, gives a Hubble constant of 65 ± 8 km s^{-1} Mpc^{-1}.

Acknowledgments
We are particularly grateful to J. Secker for the use of his maximum likelihood code and useful suggestions. We also thank C. Grillmair for helpful discussions. This research was funded by the HST grant GO-05920.01-94A

Note added in proof
After finishing this paper, we became aware of the I band surface brightness fluctuation measurements of NGC 5846 which gave (m–M) = 32.11 ± 0.10 (Blakeslee & Tonry 1996, personal communication). For $V_{CMB} = 1883$ km s^{-1}, this corresponds to $H_\circ = 71 \pm 4$ km s^{-1} Mpc^{-1}. These values are within the errors of our measurement.

References

Aguliar, L., Hut, P., & Ostriker, J. P. 1988, ApJ, 335, 720

Ashman, K. M., Conti, A., & Zepf, S. E. 1995, AJ, 110, 1164

Baum, W. A., *et al.* 1995, AJ, 110, 2537

Biermann, P. L., Kronberg, P. P., & Schmutzler, T. 1989, A & A, 208, 22

Burrows, C., *et al.* 1993, Hubble Space Telescope Wide Field and Planetary Camera 2 Instrument Handbook, STScI

Couture, J., Harris, W. E., & Allwright, J. W. B., 1990, ApJS, 73, 671

Faber, S. M., *et al.* 1989, ApJS, 69, 763

Forbes, D. A. 1996a, AJ, in press

Forbes, D. A. 1996b, AJ, in press

Forbes, D. A. 1997, in preparation

Forbes, D. A., Elson, R. A. W., Phillips, A. C., Illingworth, G. D. & Koo, D. C. 1994, ApJ, 437, L17

Forbes, D. A., Franx, M., Illingworth, G. D., & Carollo, C. M. 1996, ApJ, 467, 126

Freeman, W. L. *et al.* 1994, ApJ, 427, 628

Grillmair, C. J. 1995, personal communication

Harris, W. E. 1991, ARAA, 29, 543

Holtzman, J., *et al.* 1995, PASP, in press

Holtzman, J., *et al.* 1996, PASP, submitted

Jacoby, G. H., *et al.* 1992, PASP, 104, 599 (J92)

Kelson, D. D. *et al.* 1996, ApJ, 463, 26

Mould, J. R. *et al.* 1995, ApJ, 449, 413

Murray, S. D., & Lin, D. N. C. 1992, ApJ, 400, 265

Perelmuter, J. L., Brodie, J. P., & Huchra, J. P. 1995, AJ, 110, 620

Sandage, A., & Tammann, G. A. 1995, ApJ, 446, 1

Secker, J. 1992, AJ, 104, 1472

Secker, J., & Harris, W. E. 1993, AJ, 105, 1358 (SH93)

Stetson, P. B., 1987, PASP, 99, 191

Whitmore, B. C., Sparks, W. B., Lucas, R. A., Macchetto, F. D., & Biretta, J. A. 1995, ApJ, in press (W95)

Fig. 1.— Grey scale WFPC2 image (see attched jpeg image) of a ~ 40″ × 40″ area located ~ 2 ′ from NGC 5846. The selected globular clusters are indicated by black squares. The galaxy is located in the upper left direction.

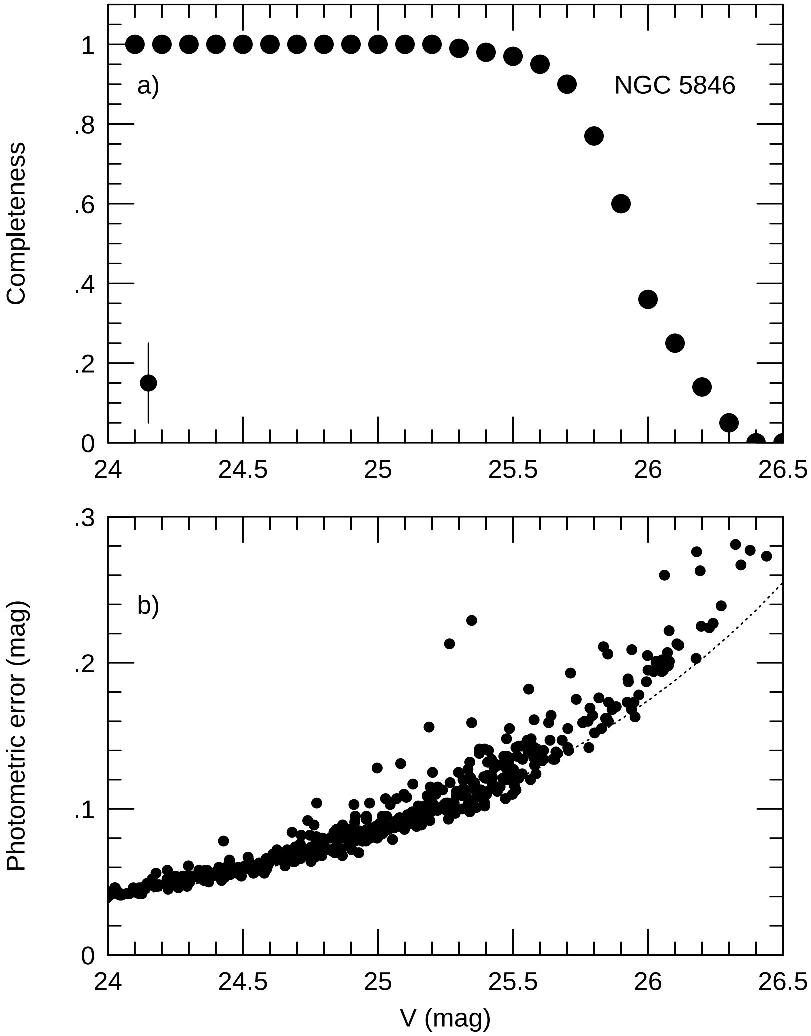

Fig. 2.— Completeness function for GC from simulations. Circles show the fraction of simulated GCs detected in 0.1 magnitude bins. A typical error bar is shown in the lower left. Brighter than V = 25, the value is fixed to 1.0. **b)** Photometric error as a function of GC V magnitude determined from DAOPHOT. Circles show the data points, and the dashed line an exponential fit to the data of the form p.e. = exp [a (V − b)].

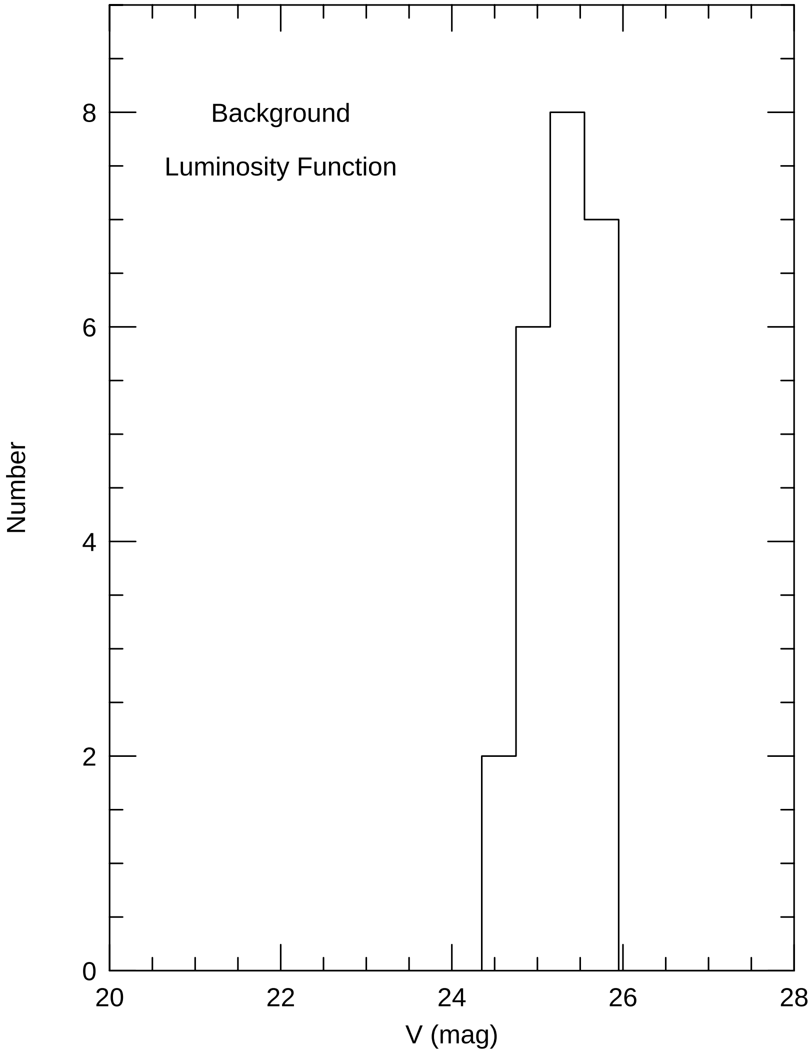

Fig. 3.— Luminosity function of unresolved background sources in a single high Galactic latitude 2400 sec WFPC2 image from the Medium Deep Survey (Forbes *et al.* 1994). Sources have been detected using the same parameters as the globular cluster data.

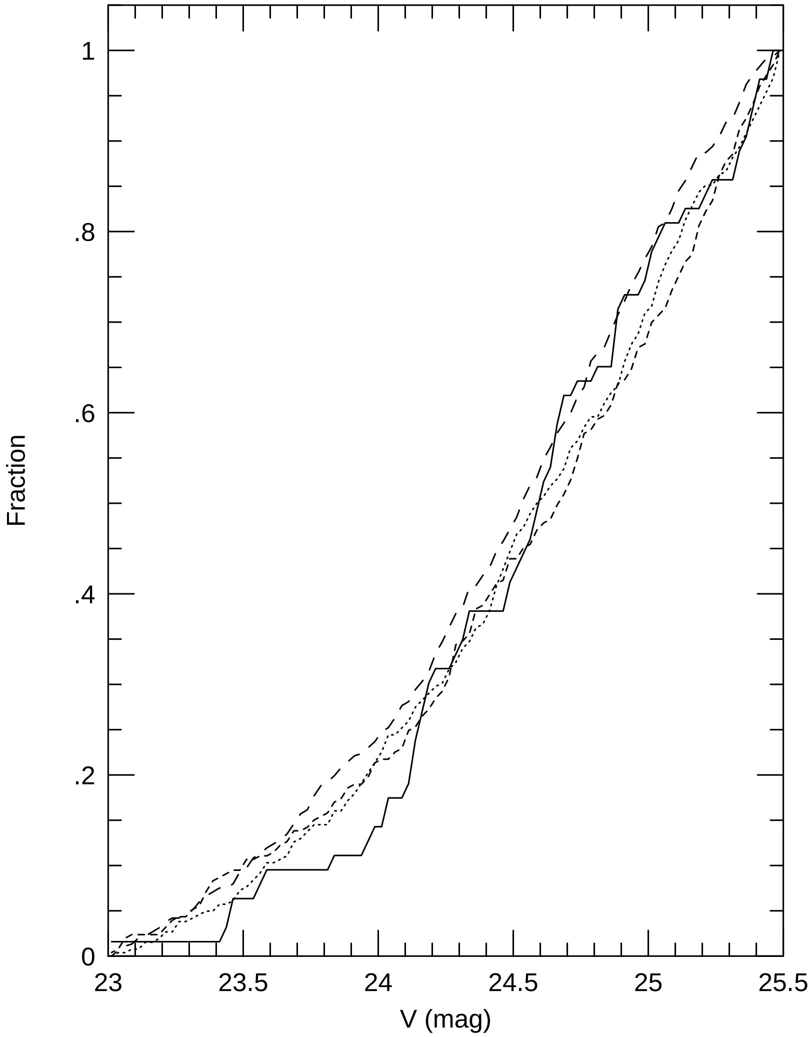

Fig. 4.— Detection of actual globular clusters normalized at V = 25.5. The three central WFC CCDs are shown by a long dash line, the WFC CCDs of the northern pointing by a dotted line and the WFC CCDs of the southern pointing by a short dash line. The combined data of the north and south pointings for the PC CCDs (after correction for their lower point source sensitivity) are shown by a solid line. Fainter than V = 25.5 background galaxies contribute strongly. The fraction of actual detected globular clusters is similar over all three pointings (a range of ∼ 3–30 kpc).

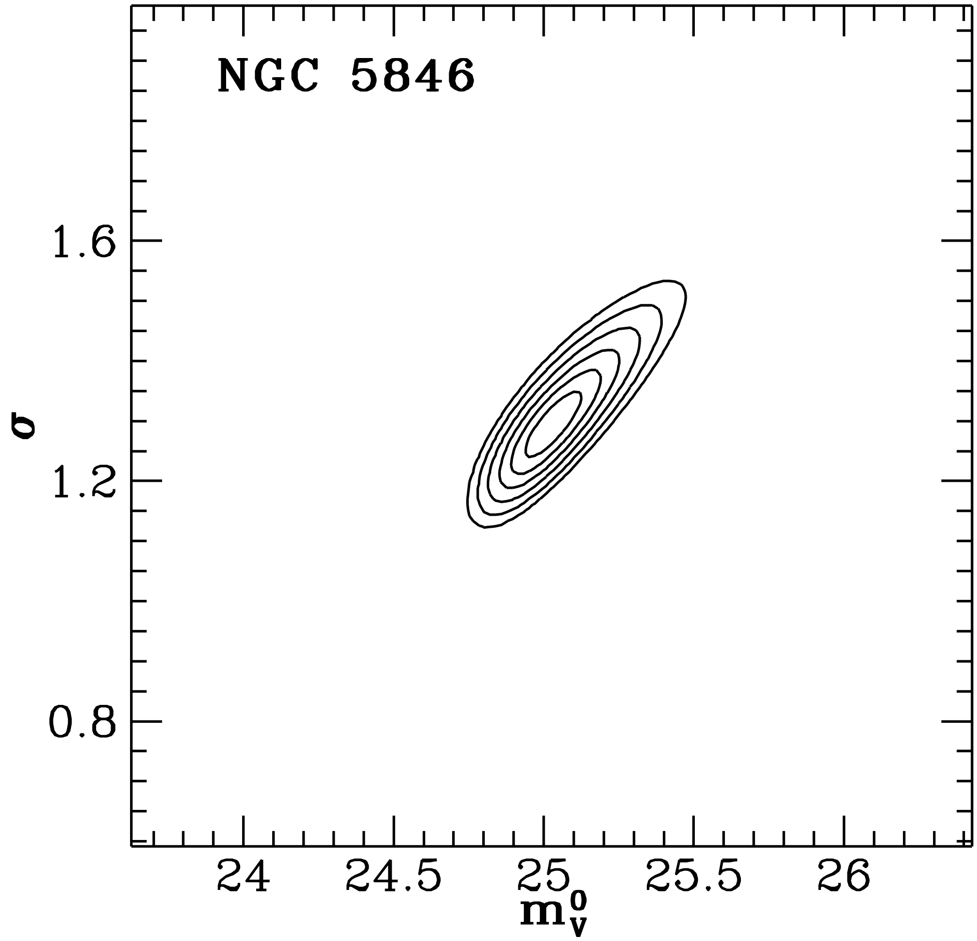

Fig. 5.— Probability contours for the turnover magnitude and dispersion for a Gaussian fit from the maximum likelihood code of Secker & Harris (1993). Contours represent 0.5 to 3 standard deviations probability limits from the best estimate (see Table 1).

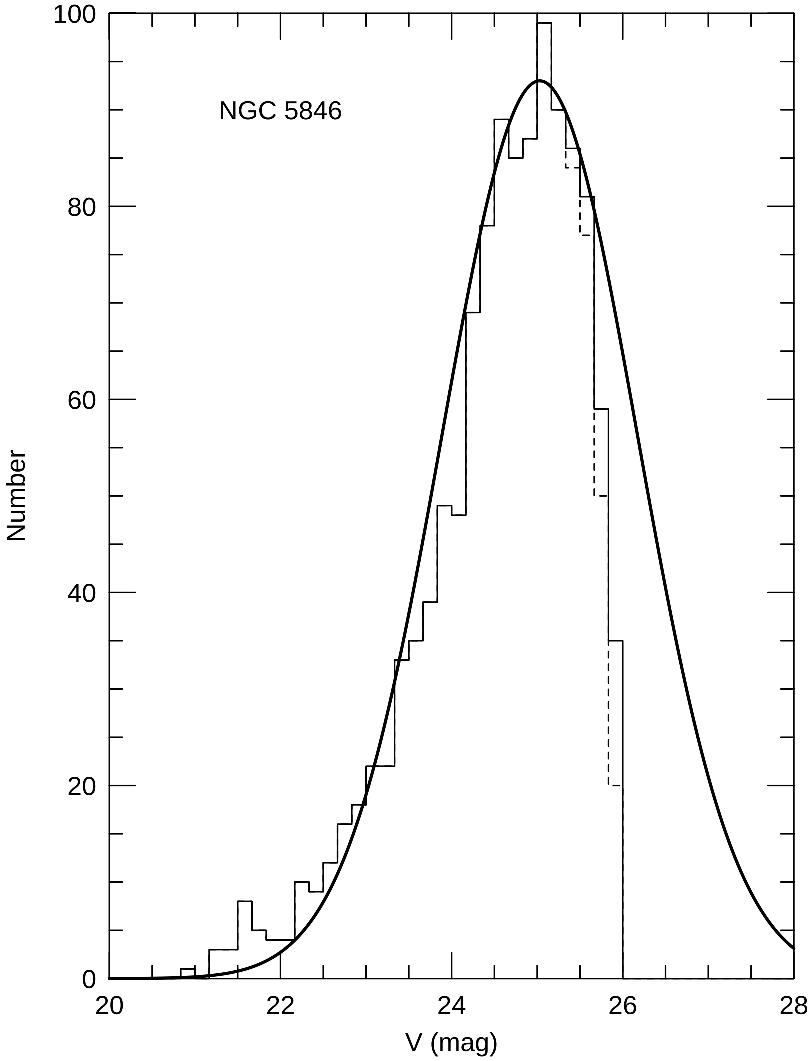

Fig. 6.— Globular cluster luminosity function for NGC 5846. The raw data are shown by a dashed line, and by a thin solid line after a completeness correction has been applied. The maximum likelihood best–fit Gaussian profile, which includes the effects of photometric error and background contamination, is superposed as a thick solid line. Note that the fitting procedure does not use binned data.

Table 1. Globular Cluster Luminosity Function Parameters

Profile (1)	m_V^0 (mag) (2)	σ (mag) (3)	(m–M) (mag) (4)
Gaussian	25.08 ± 0.10	1.34 ± 0.06	32.35 ± 0.23
t_5	25.02 ± 0.10	1.05 ± 0.06	32.29 ± 0.23

Notes to Table 1.

(1) Profile for GCLF fit; (2) Apparent magnitude of the GCLF turnover; (3) Dispersion of the GCLF; (4) Distance modulus assuming $M_V^0 = -7.62 \pm 0.2$ and a metallicity correction of 0.35.

This figure "plate1.jpg" is available in "jpg" format from:

http://arXiv.org/ps/astro-ph/9611141v1